

# Simulations of common envelope evolution in triple systems: Circumstellar case

Hila Glanz<sup>1</sup> \* and Hagai B. Perets<sup>1</sup>

<sup>1</sup>*Technion - Israel Institute of Technology, Haifa, 3200002, Israel*

Accepted 2020 October 14. Received 2020 October 14; in original form 2020 March 31

## ABSTRACT

The dynamical evolution of triple stellar systems could induce the formation of compact binaries and binary mergers. Common envelope (CE) evolution, which plays a major role in the evolution of compact binary systems, can similarly play a key role in the evolution of triples. Here we use hydrodynamical simulations coupled with few-body dynamics to provide the first detailed models of triple common envelope (TCE) evolution. We focus on the circumstellar case, where the envelope of an evolved giant engulfs a compact binary orbiting the giant, which then in-spirals into the core of the evolved star. Through our exploratory modeling we find several possible outcomes of such TCE: (1) The merger of the binary inside the third star’s envelope; (2) The disruption of the in-spiraling binary following its plunge, leading to a chaotic triple dynamics of the stellar-core and the two components of the former disrupted binary. The chaotic evolution typically leads to the in-spiral and merger of at least one of the former binary components with the core, and sometimes to the ejection of the second, or alternatively its further now-binary common-envelope evolution. The in-spiral in TCE leads to overall slower in-spiral, larger mass ejection and the production of more aspherical remnant, compared with a corresponding binary case of similar masses, due to the energy/momentum extraction from the inner-binary. We expect TCE to play a key role in producing various types of stellar-mergers and unique compact binary systems, and potentially induce transient electromagnetic and gravitational-wave sources.

**Key words:** stars: evolution – hydrodynamics – stars: mass-loss – (stars:) binaries (including multiple): close

## 1 INTRODUCTION

Triple systems are frequent among stellar systems, and in particular massive systems (e.g. [Toonen et al. 2016](#); [Moe & Di Stefano 2017](#), and references therein), and their evolution may lead to a wide variety of non-trivial and sometimes exotic outcomes. These include the formation of various types of compact stellar binaries and triples, stellar mergers, and the possible triggering of transient events (e.g. [Eggleton & Verbunt 1986](#); [Iben & Tutukov 1999](#); [Ford et al. 2000](#); [Soker 2004](#); [Perets & Fabrycky 2009](#); [Thompson 2011](#); [Perets & Kratter 2012](#); [Hammers et al. 2013](#); [Tauris & van den Heuvel 2014](#); [Sabach & Soker 2015](#); [Naoz 2016](#); [Di Stefano 2019](#)). Although triple stellar systems had been extensively studied, the vast majority of the studies focused on the dynamical evolution of such systems; either through short-term dynamical evolution of unstable systems, or the longer-term secular evolution of triples (e.g. [Valtonen & Karttunen 2006](#); [Naoz 2016](#), and references therein). Few studies explored the implications of mass-loss and/or mass transfer in stellar triples ([Iben & Tutukov 1999](#); [Soker 2004](#); [Perets & Kratter 2012](#); [Shappee & Thompson 2013](#); [de Vries et al. 2014](#); [Michaely & Perets 2014](#); [Hillel et al. 2017](#); [Stefano 2018](#);

[Portegies Zwart & Leigh 2019](#); see [Toonen et al. 2016](#) for an overview), but a detailed modeling of the triple common envelope (TCE) phase, and in particular fully hydrodynamical simulations of this phase had not yet been explored, to the best of our knowledge, and are the focus of our study.

Binary common envelope (CE) results from an unstable Roche-lobe overflow in a binary system, most typically following the evolution of one of the binary components and the extension of its envelope during the red giant (RG) phase. The binary components are thought to in-spiral inside the (now shared) CE, leading to the shrinkage of the orbit, on the expense of the outer envelope expansion and possible ejection. CE evolution (CEE) is believed to be one of the most important steps in the evolution of close binaries, providing an essential part in the formation of compact binaries and stellar mergers ([Paczynski 1976](#); [Izzard et al. 2012](#); [Ivanova et al. 2013](#); [Soker 2017](#), and references therein).

A circumstellar TCE occurs when a more-compact binary (hereafter binary<sub>2–3</sub> as presented in Figure 1), or the inner-binary, as it is termed in the context of hierarchical triples) orbits an evolved star which fills its Roche-lobe (see middle panel of Figure 1). Then, similarly to the binary CE case, if the mass-transfer is unstable, a shared envelope is formed. The evolution in this case will be somewhat different due to the potential additional energy input from the binary<sub>2–3</sub> system and/or the more complex and potentially chaotic dy-

\* E-mail: glanz@tx.technion.ac.il

namics of the (possibly unstable) triple. Moreover, the motion and evolution of binary<sub>2-3</sub> could be affected by the interaction with the giant’s gaseous envelope. As we discuss in the following, the outcome of such process can be a merger of the giant’s core with one or more of the companions, a merger of binary<sub>2-3</sub>’s components, or a tidal disruption of the binary and the possible ejection of one of the stellar components. The different evolution could also induce a different structure of the remnant planetary nebulae around the resulting system (Soker et al. 1992).

A TCE could also involve a different, circumbinary configuration. In this case a binary CE is formed in a system with a distant third companion, i.e. the evolved star is now part of an inner binary, orbited by an outer third component. The expansion of the envelope during the binary CE may then lead to engulfment of the third companion, and its potential in-spiral onto the binary in a TCE. Here we focus on the circumstellar case; the circumbinary case will be explored elsewhere.

Past hydrodynamical simulations of binary CEE encountered major difficulties; they show that following the in-spiral phase most of the envelope is not ejected, but only expands to larger size while still remaining bound to the binary (e.g. Ricker & Taam 2012; Ivanova et al. 2013, 2015; Kuruwita et al. 2016; Ohlmann et al. 2016; Iaconi et al. 2017). Consequently, other physical processes have been suggested as possible causes for its ejection; these include jets launching inside the CE (Shiber et al. 2019; Schreier et al. 2019), long period pulsations (Clayton et al. 2017) and dust driven winds (Glanz & Perets 2018). Other suggested the importance of including the recombination energy (Ivanova et al. 2015), but this is doubtful as being the sole reason for the ejection- (Grichener et al. 2018) as well as for explaining formation of wide post-CE binary systems (Reichardt et al. 2020). In this paper we are not aiming to solve those problems, but only on the comparison between the outcomes of the CEE of binary and triple systems.

The paper is structured as follows. We first describe our simulation methods in the following section. We then present our results (section 3) and possible outcomes of circumstellar TCE, discuss them in section 4, and summarize.

## 2 METHODS

In our models we simulate the dynamical evolution of an evolved triple system in which a binary system orbits a more massive red giant (which we term the circumstellar case). The giant’s envelope engulfs the binary, leading to the binary’s in-spiral into the giant envelope and producing a triple common envelope (TCE) configuration. For this purpose, we first modeled a red-giant star using the MESA 1D stellar evolution code (Paxton et al. 2011) (version 2208), and then mapped its density profile into a 3D model to be used in the hydrodynamical code GADGET2 (Springel 2005). After relaxing the star in the hydrodynamical code, we coupled the star to an outer-orbiting binary (binary<sub>2-3</sub>; modeled as two point mass stars, unlike the fully hydro-modeled giant star, and coupled the hydro model with a higher resolution dynamical code).

We use the AMUSE - Astrophysical Multi-purpose Software Environment (Portegies Zwart et al. 2009) as a platform for coupling between several external codes used

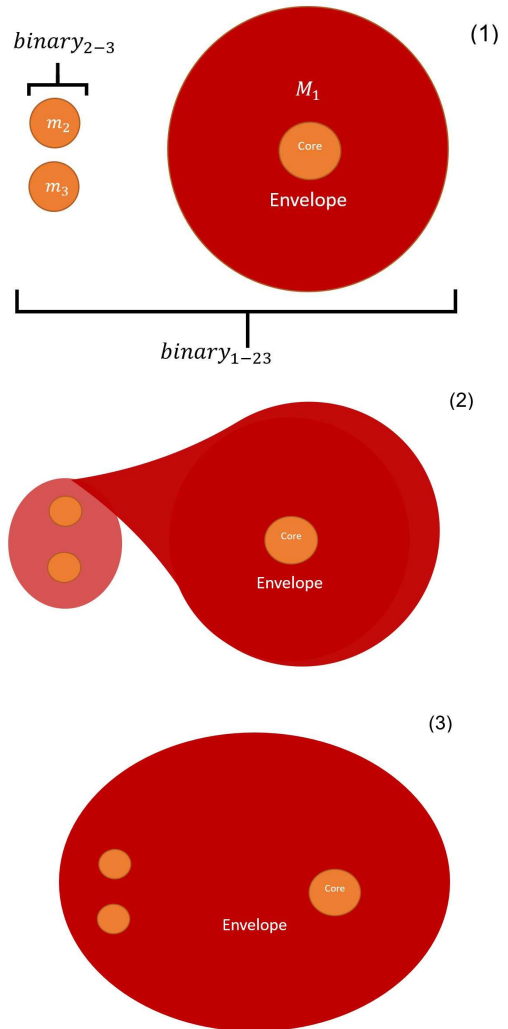


**Figure 1.** A schematic drawing of a circumstellar triple common envelope phase. The first stage introduces a hierarchical triple system prior to the Roche-lobe overflow, where a red-giant star is in orbit with a compact binary (binary<sub>2-3</sub>). The second and third stages demonstrate the Roche-lobe filling of the triple system, and the triple common envelope, respectively.

for the physical processes. In particular, we used MESA (Paxton et al. 2011), the stellar evolution code, in order to produce the initial profile of the RG star. The dynamics of the stars of binary<sub>2-3</sub> is modeled by the dynamical code HUAYNO (Pelupessy et al. 2012) which is a N-Body code, and the gravitational influence of binary<sub>2-3</sub> on the envelope is modeled by MI6 (Fujii et al. 2007). In the following we provide a more detailed description of the different parts of our model.

### 2.1 Modeling the giant gaseous envelope and core

#### 2.1.1 Stellar evolution

The initial giant model is created with the stellar code MESA (Paxton et al. 2011). We create the initial model by simulating the stellar evolution of a star from the zero-age main sequence stage up to the red-giant stage. Here we explored

cases where the giant reached its maximal radius (if it were to evolve in isolation) when the TCE stage ensues. We run MESA within the AMUSE framework. This allows us to better control the stopping condition by running the evolution step by step. Furthermore, the final model can then be simply coupled with the other few-body modeling components discussed above. We considered two possible masses for the primary red-giant, an  $8M_{\odot}$  case and a  $2M_{\odot}$  case. In both cases we evolved the primary star up to the red giant (RG) phase. The giant with  $8M_{\odot}$  was evolved until it reached a radius of  $R_{\star} \approx 0.5AU \approx 110R_{\odot}$ . Its hydrogen-exhausted core is approximately  $M_{\text{core}} \approx 1.03M_{\odot}$  with a core radius of  $R_{\text{core}} \approx 0.09R_{\odot}$ . Its dynamical time scale is  $\approx 5.5$  days and the thermal time scale  $\approx 5160$  years. The radial profiles of the evolved model are presented in Figure 2. The  $2M_{\odot}$  giant was evolved until it reached a radius of  $R_{\star} \approx 50R_{\odot}$ . Its core-size was found to be approximately  $M_{\text{core}} \approx 0.36M_{\odot}$  with a core radius of  $R_{\text{core}} \approx 0.015R_{\odot}$  (similar to the model simulated by Ohlmann et al. 2016). Its dynamical time scale is  $\approx 3.3$  days and the thermal time scale  $\approx 4500$  years.

### 2.1.2 Smoothed particle hydrodynamics simulation

We use the GADGET2 (Springel 2005) smoothed-particle hydrodynamics (SPH) for the hydro-dynamical modeling. The SPH method works by dividing the fluid into a set of discrete elements, referred to as particles. These particles have a spatial distance, termed the "smoothing length", typically represented in equations by  $h$ , over which their properties are "smoothed" by a kernel function. This means that the physical quantity of any particle can be obtained by summing the relevant properties of all the particles which lie within the range of the kernel, and the contribution of each particle is weighted according to its distance from the particle of interest.

In GADGET2, the kernel function is (Monaghan 1992):

$$W(r, h) = \frac{8}{\pi h^3} \begin{cases} 1 - 6\left(\frac{r}{h}\right)^2 + 6\left(\frac{r}{h}\right)^3 & 0 \leq r \leq \frac{h}{2} \\ 2\left(1 - \frac{r}{h}\right)^3 & \frac{h}{2} \leq r \leq h \\ 0 & h < r \end{cases}$$

where  $r$  is the relative distance between the two particles and  $h$  is the smoothing length of the particle. One should note that the smaller is the smoothing length, the smaller is the number of neighbors that should be taken into account for the calculation of each SPH particle. Another important parameter is the softening length, which keeps the simulation from non-physical behavior at very small separations between the point-mass particle and other particles, either point-mass or SPH particles. The gravitational potential of such particles is then

$$\phi = \frac{GM}{|\Delta r^2 + \epsilon^2|^{\frac{1}{2}}},$$

where  $M$  is the mass of one point-mass particle,  $\Delta r$  is the distance between the particle and the given location, and  $\epsilon$  is the softening length. In cases (like ours), where the simulation uses the softening length for smoothing the kernel,  $\epsilon$  can be thought as the radius of the point-mass particle.

### 2.1.3 Mapping the stellar model into the SPH model

**2.1.3.1 Mapping:** The core of a giant star is much denser than its outer envelope, and is not resolved in our simulations. Our focus here is not on modeling physical mergers and interactions with the small and unresolved dense core, but rather exploring the interactions with the stellar envelope. We therefore represent the core in our simulations as a point mass particle (called "dark matter particle" in Gadget2, because of their application to cosmological simulations) without considering changes in its internal structure. We chose the softening length such that the potential of the core is approximately its analytical form at distances larger than  $2.8\epsilon$ ,  $\epsilon \approx 10r_c$ , where  $r_c$  is the radius of the hydrogen-exhausted core, inducing the potential of a Plummer sphere of size  $\epsilon$ .

To convert the stellar model created by MESA into a 3D SPH model, we used AMUSE's function `Star_to_sph` (Portegies Zwart & McMillan 2018). This function converts the core region into a point mass particle with an effective radius as described above, and corrects the density and internal energy profiles to maintain pressure equilibrium and conserve the original entropy profile (as explained in de Vries et al. 2014). It then divides this external region to our desired number of particles, with equal masses and different smoothing lengths. Each gas particle has its own gravitational potential and can interact with its surrounding, i.e. we use the Lagrangian form of the fluid equations of motion.

**2.1.3.2 Relaxation:** Following the mapping of the 1D model from MESA to 3D, and the use of somewhat different equation of state between the codes (the 1D radial OPAL EOS in MESA, which is explained in Paxton et al. 2011 and 3D hydrodynamical equations in Lagrangian form in Gadget2, as described in Springel 2005), a relaxation stage is required as to obtain a stable stellar configuration for the SPH model. During this stage, we keep the center of mass (COM) position and COM velocity constant; we adiabatically adjust the position and velocity of each SPH particle for 130 days  $\approx 24$  dynamical times (for our more massive giant). The particle positions and velocities are adjusted after each step in the following way

$$r_{i,j} = (r_{i,j} - r_{COM,i}) + r_{COM,0}$$

$$v_{i,j} = (v_{i,j} - v_{COM,i}) \cdot (i/nsteps) + v_{COM,0},$$

Where  $r_{i,j}$  and  $v_{i,j}$  are the  $j$ 'th gas particle position and velocity at step  $i$ ,  $r_{COM,i}$  and  $v_{COM,i}$  are the giant's center of mass position and velocity at step  $i$ ,  $nsteps$  is the total number of the damping steps. After each step the internal velocities are damped by a factor which decreases from 1 in the first step to 0 in the last one.

We first test the stability of our massive giant star model in isolation. For this purpose, we used a similar method as described in Iaconi et al. (2017). Following a damping phase as described above, we continued the evolution of the giant for an additional 130 days (same amount of dynamical times) with no damping. At each time step we compared the gas particle velocities with some typical velocity scales: the local sound speed,  $c_s$ , the initial velocities of binary<sub>2-3</sub>'s components, relative to the center of mass of the giant, and the escape velocity,  $v_{esc} = R_{\star}/t_{dyn}$ , where  $R_{\star}$  and  $t_{dyn}$  are the initial star radius and dynamical time, respectively. During

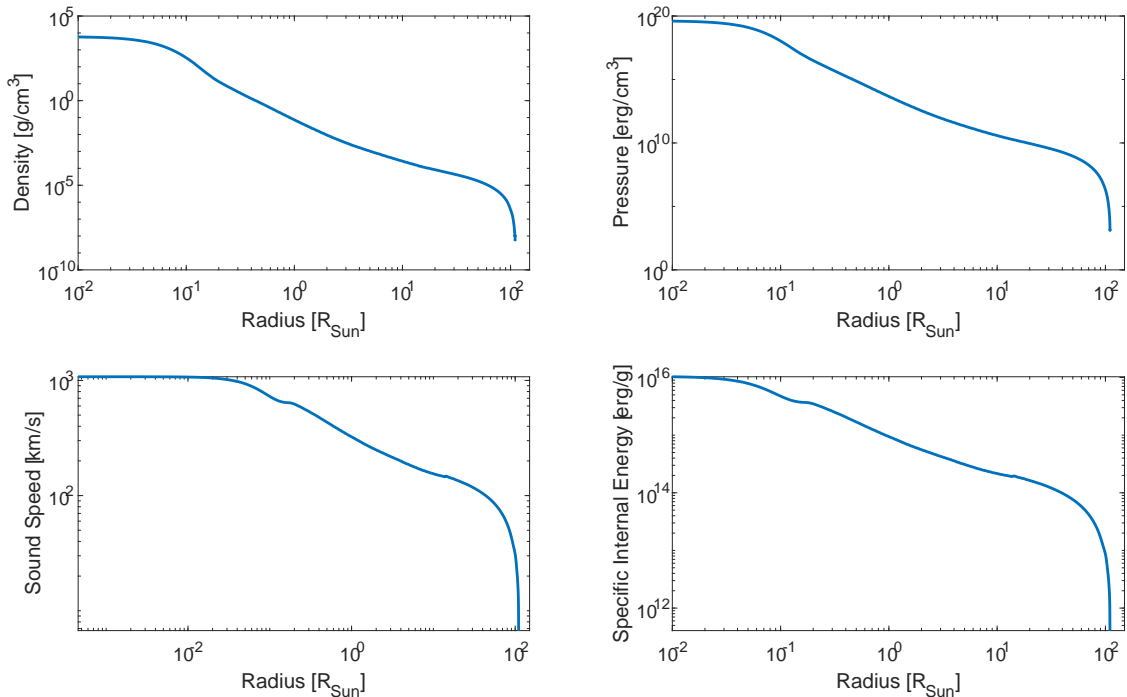


**Figure 2.** Radial profiles of the evolved  $8M_{\odot}$  stellar model

those  $\sim 24$  dynamical time scales, at most 0.05 percent of the particle exceeded the lowest of those velocity limits.

Since the star is stabilized in isolation, we could add the gravitational field of  $\text{binary}_{2-3}$  during the damping phase and form a binary (trinary) system which is less affected by the sudden change in the potential, and by the change of the simulation code. More precisely, We follow the same method as mentioned above, but we now include the gravitational potential of  $\text{binary}_{2-3}$ . We do not allow the binary to evolve during that time (i.e, it is considered as a constant potential at this stage), where we follow the same approach as [de Vries et al. \(2014\)](#).

While taking the companion into account during the relaxation stage, we place it far enough from the giant such that it won't considerably affect the giant's shape (nor initiate a RLO), but sufficiently near such that the system will eventually enter the CE stage during the simulation time. The result of such configuration is a "gradual" addition of the gravitational potential of the companion, which is more natural than its sudden inclusion where it has a greater effect.

## 2.2 Coupling of the red-giant with the inner (point masses) $\text{binary}_{2-3}$

The motion of the system of the  $\text{binary}_{2-3}$  is a classical 2-body problem, which is perturbed by the gravitational potential of the core and the envelope of the giant star. In order to improve the model accuracy of the binary orbital motion and the momentum conservation, we make use of the HUAYNO code ([Pelupessy et al. 2012](#)), which is a special class of Individual Time-step Scheme, semi-symplectic direct N-body integrator. The giant star gaseous envelope is modeled us-

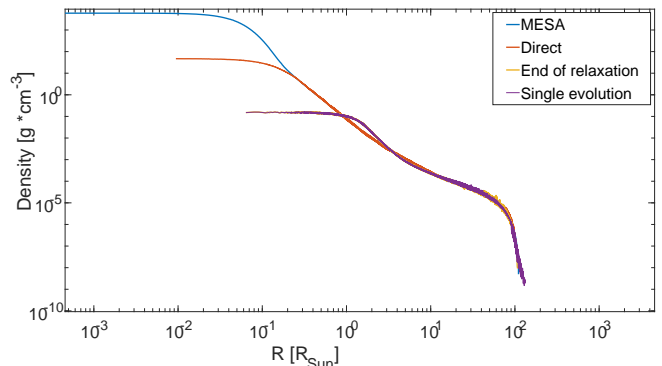


**Figure 3.** Radial density profiles of the evolved  $8M_{\odot}$  stellar model, before mapping to a 3-D model (blue); immediately following the mapping (orange); after the damping phase (yellow); and following the later evolution in isolation (purple).

ing the SPH code Gadget2 as discussed earlier. The N-body code is coupled with the SPH code using the AMUSE environment. We effectively split the Hamiltonian into the different parts, which are modeled using the different codes. This combination can give us better approximation for each of the sub-systems. The two sub-systems are then linked through an AMUSE "bridge" between  $\text{binary}_{2-3}$  and the gas using the MI6 code ([Fujii et al. 2007](#)); a 6th order N-Body integrator with mixed 4th and 6th order Hermite integration scheme, originally developed for simulating the galactic center. Like in the galactic center, we have a multiple system ( $\text{binary}_{2-3}$ ) affected by the gravitational potential of the third star core and its gaseous envelope (calculated with Gadget2), and affecting the envelope evolution. Overall we follow a similar approach

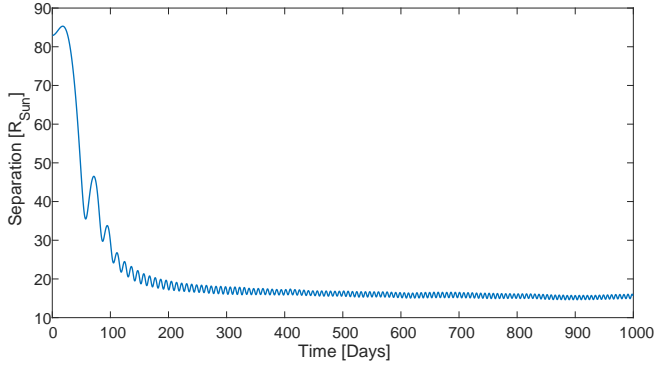


**Figure 4.** Simulation 16 (see 1, with similar configuration to Passy et al. 2012, of  $1M_{\odot}$  giant with  $0.6M_{\odot}$  companion. This simulation was done in order to benchmark and test the use of Gadget2 (Springel 2005) for fully simulating common envelope evolution, not done previously, to the best of our knowledge. We find our simulation well reproduces previous simulations done with other codes (compare with Passy et al. 2012), showing similar evolution timescales and kinematics, both in the rapid inspiral stage and later during the slower evolution, and giving rise to similar final separations.

as used by de Vries et al. (2014) to study mass-transfer dynamics in triple systems (that are not evolving through TCE phase).

### 2.3 Code bench-marking and resolution

In order to test our code, we first successfully reproduced the simulated evolution of previously studied binary common envelope and triple mass-transfer systems (Passy et al. 2012-see Figure 4, and de Vries et al. 2014, respectively). We carry out resolution tests in the limits of long computational times, with several TCE models, at progressively higher resolution, up to 500K. We found that the use of 250K SPH particles produced similar results compared with higher resolution simulations (500K) and we use this resolution throughout the models discussed below (See Figure 5 ). Our models with 100K, 250K and 500K show consistent results. Nevertheless, higher resolution simulations are desired in order to confirm the convergence. Given the high computational cost needed for higher resolution simulations, we resort to the current resolution allowing us to model a reasonable phase space, of models with our available computational power. These resolutions compare well with most currently-run cutting-edge simulations of CEE.

All models were running on the Astric computer cluster of the Israeli I-CORE center, with up to 32 cores used in each run. Even with these computational resources, each of the TCE simulations with more than 250K particles required over than a month to run.

We examined the resolution of our models by comparing the histogram of the different smoothing lengths throughout the envelope in our model (simulation 1 in Table 1), and its distribution at different simulation times (see Figure 6). Since most of the SPH particles in this resolution had much smaller smoothing length than the orbit of the binary<sub>2-3</sub>, the gas interaction can affect binary<sub>2-3</sub> even in the outer region, where the resolution is the lowest (see bottom of same Figure 6). In addition, the distribution of the smoothing lengths in

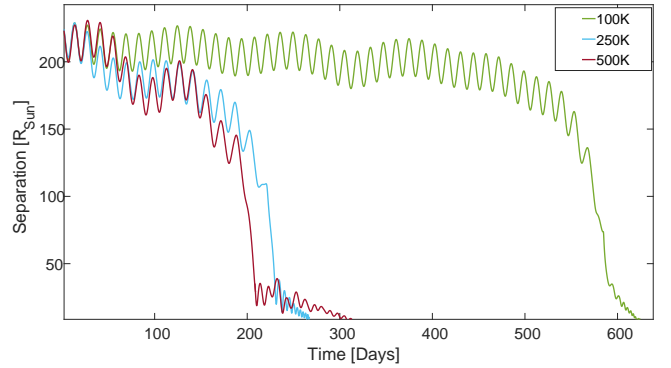


**Figure 5.** Separation between the giant’s core and the companion which will finally merge in simulation 1 (see Table 1) that was ran with 3 different resolutions, i.e- different number of SPH particles. We can see that the runs with 250K and 500K particles have relatively similar initiation time of the fast plunge-in and in the overall duration until merging with the core. The plunge-in phase began much later in the run consisted of 100K particles, but then had a faster duration. Overall, the outcomes were the same in all of those simulations- one of the companions merged with the core, while the other one remained bound at a closer distance than prior to the CE, but did not merge.

the dense region, close to the core, varies only slightly during the simulation. Since our current focus is not the mass ejection from the outer layer, we can neglect those resolution variations. The components of binary<sub>2-3</sub> are modeled as point masses, and have no softening length affecting their mutual interaction (modeled with HUAYNO code), but their interaction with the gas and the stellar core is smoothed with  $\epsilon \approx 10r_c$ , the same value as that of the core particle (which has a similar mass). We should note, however, that due to the relatively close values of the compact binary separation and the average local smoothing length of the gas, this resolution is not sufficient for an explicit determination of the boundary between initial separations of binary<sub>2-3</sub> that lead to their mutual merger, and those that end with their disruption.

Figure 7 shows that our simulation conserved energy and angular momentum to less than 1 percent. The bottom panel shows the angular momenta components relative to the center of mass of the entire system. As expected from the onset of the CE, the angular momentum of the outer binary (binary<sub>1-23</sub>, i.e - binary<sub>2-3</sub> components’ center of mass with the giant) decreases and the envelope’s angular momentum increases as a consequence.

The duration of the relaxation stage and the CE stage were chosen to be 24 times larger than a dynamical time of 5.5 days. After a few simulations using sink particles (to measure the accreted mass on a particle), accretion on the companion and core was found to be negligible compare to their mass, in agreement with Passy et al. (2012). For that reason, we neglect any accretion effects. Some studies suggest feedback from accretion outflows/jet may affect the evolution (e.g Sabach et al. 2017; Schreier et al. 2019; Soker 2020, and references therein); the potential importance of such effects, is still debated and are beyond the scope of the current study.

Finally, we also compared the results of a TCE with a binary common envelope evolution where binary<sub>2-3</sub> component in the TCE was replaced by a single star of the same total mass, as to compare, at some level, triple and binary common

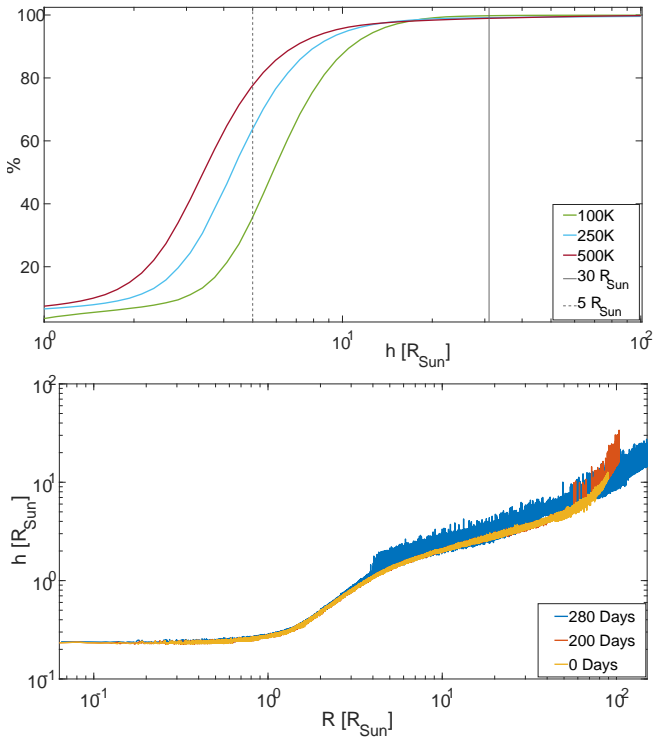


**Figure 6.** Upper Panel: Comparison between the different smoothing length distributions at different resolutions. The profiles were taken approximately at the beginning of the fast plunge-in. The vertical lines represent the approximate size of binary<sub>2-3</sub>, for a comparison with the gas smoothing lengths. Lower Panel: The resolution during different times of the simulation. Most of the changes in the smoothing lengths occur only at the outer parts of the expanding envelope.

envelope evolution effects on systems of similar masses and outer binary separations.

The different mass ratios between the evolved star and the companion(s) were chosen such that the corresponding binary CEs (simulations 14 and 15 in Table 1) would allow us to explore two qualitatively different outcomes; one is a merger outcome (simulation 14), whereas the other (15) results in the formation of short period binary on a stable orbit. As we show below, these final outcomes, either a core merger with one of the components or a stable orbit- do not change when replacing the companion with a binary as to form a TCE.

All simulations ran until a "merger" happened or the evolution reached 1400 days. The condition for such a merger of two point mass particles is when their relative distance is shorter than the sum of their smoothing lengths radii, after this point our simulations are no longer applicable.

### 3 RESULTS

#### 3.1 Triple common envelope outcomes

We studied a limited grid (given the computational cost) of possible configurations, and considered two different mass ratios. The first grid is for a  $8M_{\odot}$  RG with two  $1M_{\odot}$  companions, where we varied the following parameters with two possible values for each parameter, and considered all the possible combinations for a total of 8 modeled configurations.

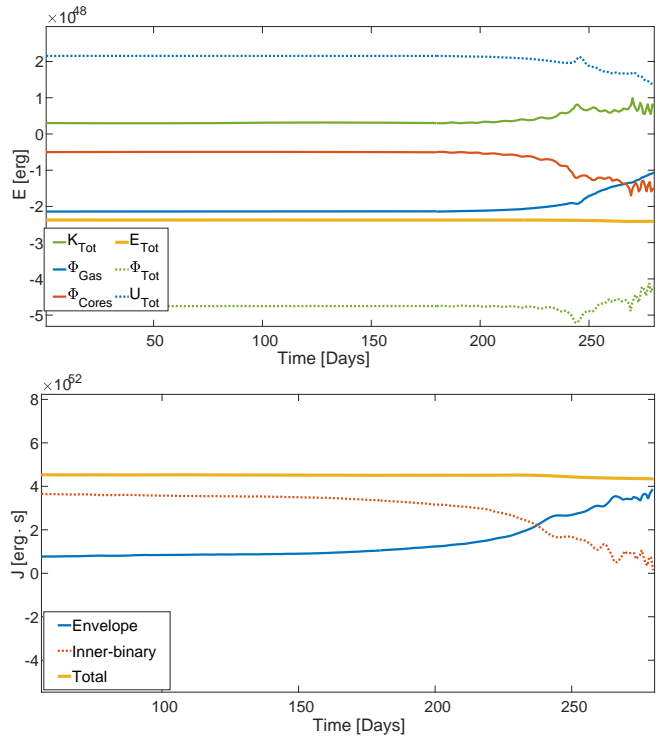


**Figure 7.** Energy and angular momentum conservation.

Upper Panel: Energy conservation as a function of time (for model 1 in Table 1). The potential energy of the outer binary (binary<sub>1-23</sub> in Figure 1) increases while the gas potential energy of the expanding envelope decreases, as well as its internal energy. The gas internal energy is the total internal energy of the system, since the components of binary<sub>2-3</sub> and the giant core are modeled as "point-mass" (gravitational only) particles. The self potential energy of binary<sub>2-3</sub> is not presented here due to its relatively small value (and thus change) during the run, in comparison with the red-giant potential. The kinetic energy at the beginning of the simulation is dominated by the energy of binary<sub>2-3</sub>, but later on the gaseous envelope gains some velocities in the outwards direction that leads to its partial unbinding.

Lower Panel: Angular momentum as a function of time. The dotted red line shows the total angular momentum of binary<sub>2-3</sub> (sum of the angular momenta of both components), the solid blue line presents the envelope's angular momentum, and the total angular momentum of the system is shown by the thick yellow line.

These parameters include (1) the initial separations; (2) the relative inclination; and (3) the orbital phases (combined with an additional  $90^{\circ}$  orbital inclination, such that binary<sub>2-3</sub> orbits the giant on a plane perpendicular to the orbital plane of the giant with the compact binary, and both companions are initially located at the same distance from the giant's core); the model parameters are listed in Table 1. In addition, we modelled three different inner separations of binary<sub>2-3</sub> for the second mass ratio of  $2M_{\odot}$  (RG) and  $0.6M_{\odot} + 0.4M_{\odot}$  companions. Overall, we simulated 11 configurations for triple systems. As mentioned above we consider only circumstellar configurations where a more compact, point-mass binary orbits an evolved star and in-spirals in its envelope. The summarized results of the evolutionary outcomes can be found in Tables 2, 3, and 4.

Initially, binary<sub>2-3</sub> is located outside the stellar envelope of the red-giant. It then progressively in-spirals due to the in-

No	Masses ( $M_{\odot}$ )	$a_{\text{out}}$ ( $R_{\odot}$ )	Inclination	$a_{\text{in}}$ ( $R_{\odot}$ )	Orbital phase
1	8 + 1 + 1	216	$5^{\circ}$	26	$0^{\circ}$
2	8 + 1 + 1	216	$5^{\circ}$	3	$0^{\circ}$
3	8 + 1 + 1	216	$45^{\circ}$	26	$0^{\circ}$
4	8 + 1 + 1	216	$45^{\circ}$	3	$0^{\circ}$
5	8 + 1 + 1	216	$5^{\circ} + 90^{\circ}$	26	$90^{\circ}$
6	8 + 1 + 1	216	$45^{\circ} + 90^{\circ}$	26	$90^{\circ}$
7	8 + 1 + 1	130	$5^{\circ} + 90^{\circ}$	26	$90^{\circ}$
8	8 + 1 + 1	130	$45^{\circ} + 90^{\circ}$	26	$90^{\circ}$
9	8 + 1 + 1	130	$5^{\circ} + 90^{\circ}$	3	$90^{\circ}$
10	8 + 1 + 1	130	$45^{\circ} + 90^{\circ}$	3	$90^{\circ}$
11	2 + 0.6 + 0.4	60	$0^{\circ}$	3	$0^{\circ}$
12	2 + 0.6 + 0.4	60	$0^{\circ}$	13	$0^{\circ}$
13	2 + 0.6 + 0.4	60	$0^{\circ}$	26	$0^{\circ}$
14	8 + 2	216	binary common envelope		
15	2 + 1	60	binary common envelope		
16	1 + 0.6	83	reproduced- Passy et al. 2012		

**Table 1.** Initial values for the modeled systems, where  $a_{\text{in}}$  is the inner separation of binary<sub>2-3</sub>. We varied the inner binary separations for both mass models, and considered different inclinations (between the orbital plain of binary<sub>1-23</sub> and binary<sub>2-3</sub>), inner-binary (binary<sub>2-3</sub>) orbital phase and outer-binary (binary<sub>1-23</sub>) separation for the high mass TCE cases. We explored a total of 10 configurations for the high mass-ratio case, and additional 3 cases for the low-mass case. In all models the evolved star is a Red Giant. The softening length of the core and binary<sub>2-3</sub> components (with respect to the giant) are  $\approx 0.9R_{\odot}$  for the high-mass cases and  $\approx 0.15R_{\odot}$  for the low-mass cases.

interaction with the stellar envelope. Figure 8 shows different snapshots of the density profile during the evolution of the CE of the first simulated scenario (see Table 1). When the binary spirals into the envelope and forms a TCE, the spiral-in becomes more rapid, the envelope expands, and mass-loss ensues mostly through the second Lagrangian point. If we compare the last snapshots with those of a corresponding (same mass) binary system (simulations 1-10 and 14 in Table 1), the shape of the surrounding gas differs significantly between the two cases (see bottom of Figure 14). The TCE case is far less symmetric than the binary CE case (see also Soker et al. 1992; Bear & Soker 2017; Schreier et al. 2019 in this regard).

When comparing cases of inner-binaries (binary<sub>2-3</sub>) with initially shorter and long periods we find that the more compact binaries we considered in-spiral more slowly than the corresponding models with longer periods (see Figures 9 and 10). The former systems are more strongly bound, and are not disrupted as they in-spiral close to the giant core; rather we find that in such cases the components of binary<sub>2-3</sub> in-spiral and merge with each other before approaching the core. Conversely, the latter, wider binary<sub>2-3</sub> in-spiral into the giant core more rapidly, and are disrupted due to the interaction with the central potential, leading to a chaotic triple dynamics of the two (former) binary<sub>2-3</sub> components and the giant’s core. The chaotic evolution can then lead to the merger of any two of the components, and the possible ejection of one of them from the system.

In Figure 9 we compare the separations between the center of mass of binary<sub>2-3</sub> and the giant’s core for the configurations initialized with  $0^{\circ}$  orbital phase. All of our simulations

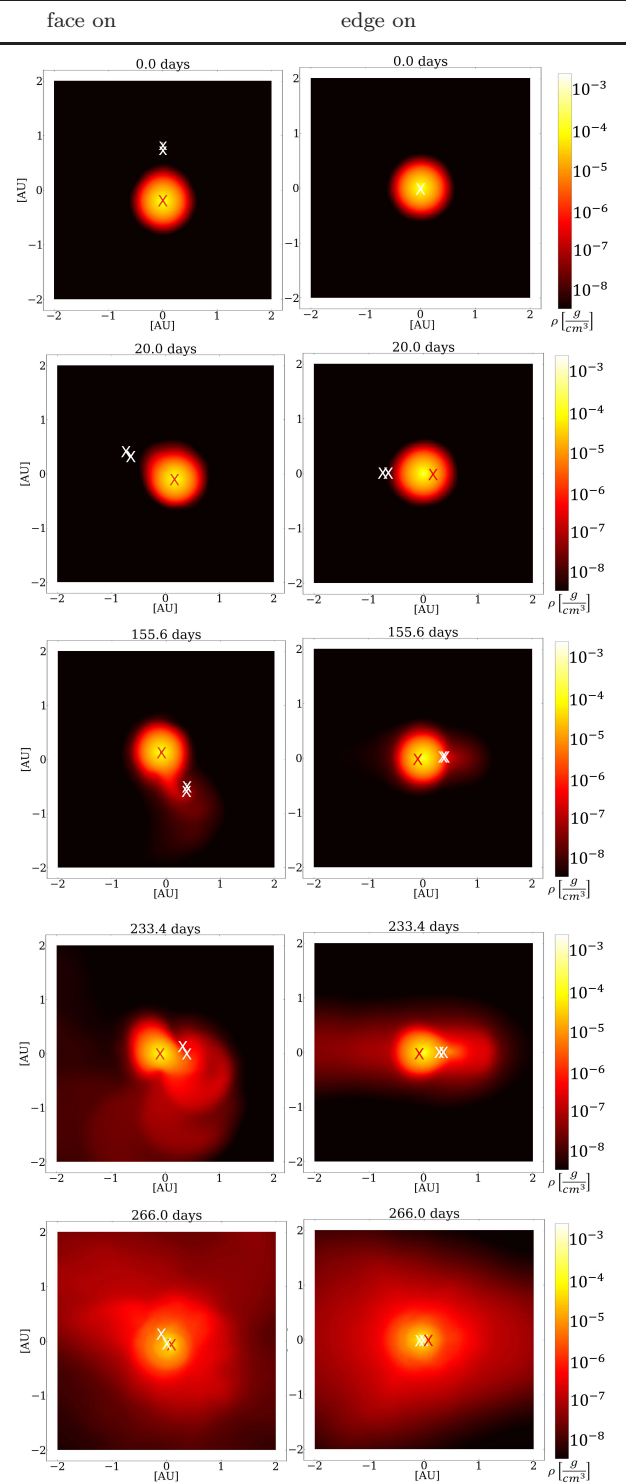


**Figure 8.** Simulation 1 in Table 1 - a common envelope evolution of an  $8M_{\odot}$  giant with an envelope radius of  $0.5\text{AU}$ , orbited by an inner-binary (binary<sub>2-3</sub>) composed of two  $1M_{\odot}$  main-sequence stars initially positioned at  $1\text{AU}$ . The left and right panels correspond to a face-on view (binary<sub>2-3</sub> moves on an anti-clockwise orbit) and an edge-on view (the binary moves towards us), respectively. The components of the binary<sub>2-3</sub> are marked with white 'X' symbols, and the giant core is marked by a red 'X' symbol. The symbol sizes do not correspond to the stellar sizes and are just shown for clarity.

of such initial zero-phase cases resulted in a core merger with one of the components of binary<sub>2-3</sub>. This suggests that the evolution is sensitively dependent on the initial closest approach of the binary closer component. The phase, and hence the initial separation of the closest binary component to the giant determine the evolution of the in-spiral, its duration and timing of both the entrance to the rapid plunge-in phase as well as the later stage of the CE, before merger. For binaries initialized with 90° inclination in respect to the orbit (orbital phase), both the stellar components are effectively initially at larger separations from the giant, and therefore show far weaker interaction at first, and required the extension of our simulation run times. Therefore, in such cases, we re-initialized these models and placed binary<sub>2-3</sub> closer to the edge of the envelope, at  $\sim 0.6$  AU. The results of this configuration can be seen in Figure 10, where, similar to the low-inclination cases, the evolution of binary<sub>2-3</sub> with smaller inner separations lead to their mutual merger before the binary approached the core.

For the two different inclinations we considered, the in-spiral process lasted much longer for the more compact binary<sub>2-3</sub> (See Figure 12). This is due to additional energy imparted to the envelope by binary<sub>2-3</sub> as its two components mutually in-spiral through their coupling to the gaseous envelope (on top of the in-spiral of the center of mass of binary<sub>2-3</sub> onto the RG core). In other words, the in-spiral of binary<sub>2-3</sub> provides an additional energy/momentum source term. The expansion of the CE is accelerated and its density decreases, consequently decreasing the dissipation and in-spiral of binary<sub>2-3</sub>'s COM onto the RG core. In both inclinations, the shorter period binary<sub>2-3</sub> resulted in an inner merger just shortly before merging with the core. In contrast, binaries with larger separation were eventually disrupted as they inspiraled close to the core.

In Figure 12 we compare the evolution of systems with different initial inner binary<sub>2-3</sub> separations (simulations 1 and 2 in Table 1, one with a wider inner binary ( $26R_{\odot}$ ) and one with a short period inner binary ( $3R_{\odot}$ ). The separation of the outer binary of the wider inner binary decreases more rapidly, and its inner separation increases when reaching the central region of the giant, leading to its disruption. The larger binding energy of binary<sub>2-3</sub> with initial shorter orbital period gives rise to a slower decrease of its outer separation, a faster dilution of the envelope (middle panel), and a weaker gravitational force on binary<sub>2-3</sub> (lower panel). As a result, the components of binary<sub>2-3</sub> merge before reaching the core of the giant.

In order to consider the sensitivity to the initial separation between the binary<sub>2-3</sub> and the giant we studied the differences between the simulations where the inner binaries (binary<sub>2-3</sub>) were positioned at 1 AU, and those initiated at 0.6 AU. Figure 11 presents the results. We find that binary<sub>2-3</sub> significantly evolves in the 1 AU models before they even reach separations of 0.6 AU, and can even merge before reaching that point. In other words, it is critical to initialize the binaries sufficiently far from the giant core as to correctly follow their evolution, as significant evolution can happen even in the early in-spiral phases (in agreement with results obtained for binary CE by [Iaconi et al. 2017](#); [Reichardt et al. 2019](#)).

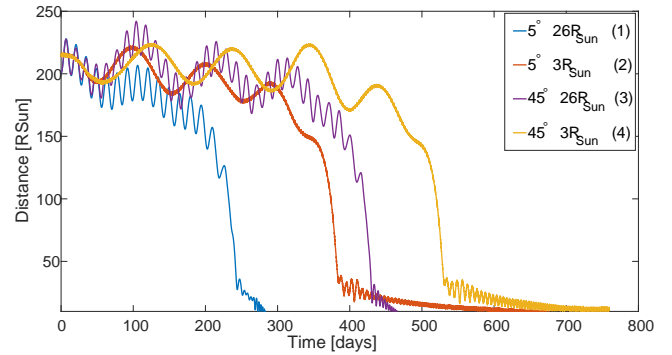


**Figure 9.** Evolution of the distance between the center of mass of binary<sub>2-3</sub> and the giant core, for simulations 1-4 (see Table 1). The plunge-in phase begins earlier in low inclination cases, due to the effective closer initial distance of one of the companions to the giant core. A shorter binary<sub>2-3</sub> separation extends the duration of the self regulated phase, because of the potential energy stored in the orbit of binary<sub>2-3</sub>

, part of which is extracted by the gaseous envelope during the in-spiral, leading to further envelope extension and mass ejection, and thereby slowing the in-spiral onto the giant core.

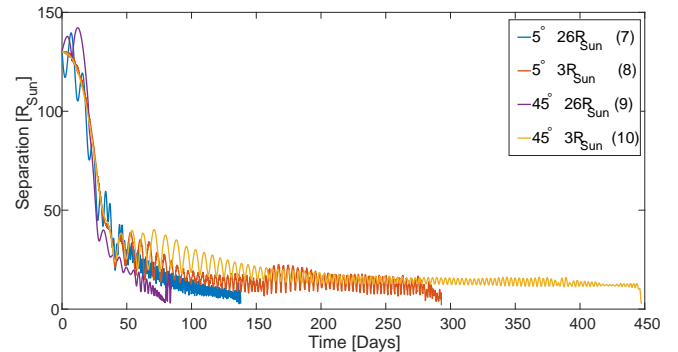


**Figure 10.** Evolution of the distance between the COM of binary<sub>2-3</sub> and the core for systems 7-10 in Table 1

, with initial 90° phase-angle (the components of binary<sub>2-3</sub> orbits their center of mass on a perpendicular plane than their mutual motion around the giant. In addition, due to the orbital phase, both companions are initially at the same distance from the giant's core).

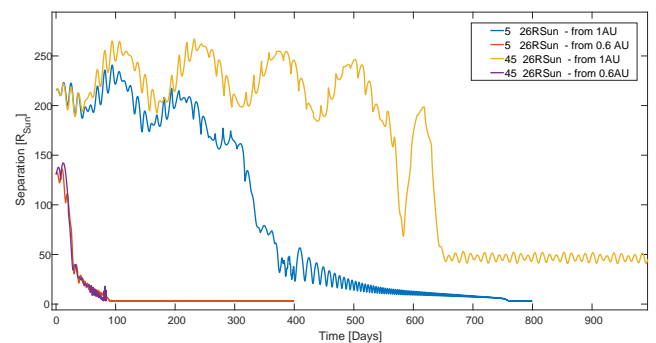


**Figure 11.** The separations between the binary<sub>2-3</sub> and the core for systems with a 90° phase, for both initial positions - at 1 AU (simulations 5,6), and 0.6 AU (7,8 in Table 1



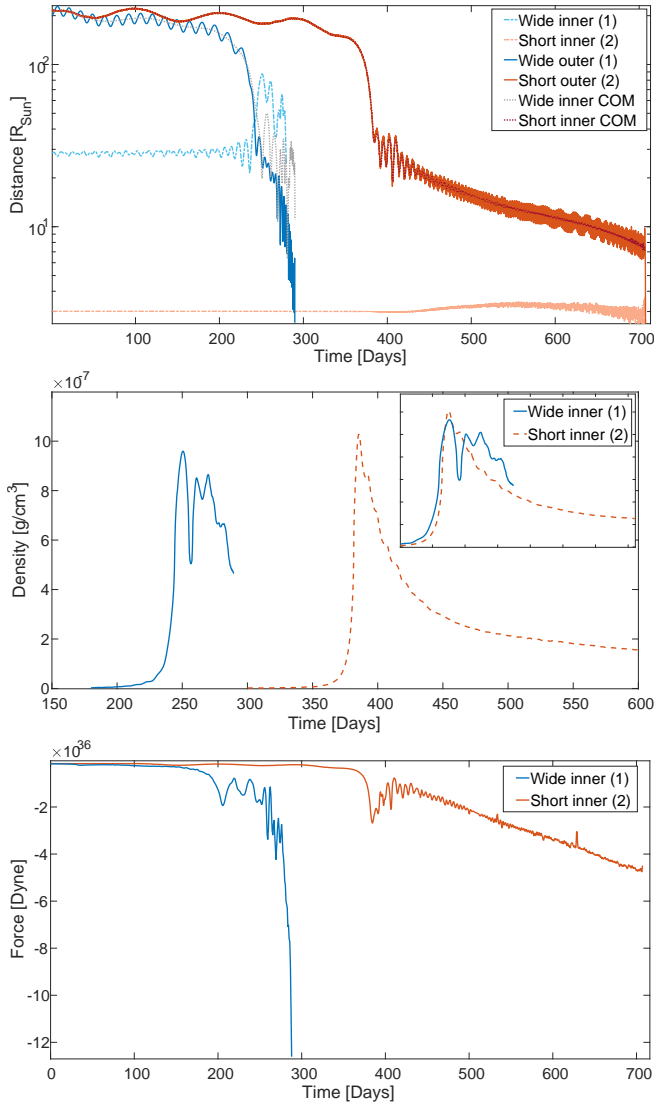


**Figure 12.** Evolution of properties of the triple components (for models 1 and 2). Upper panel: Evolution of the outer separation (binary<sub>1–23</sub>, i.e. binary<sub>2–3</sub>’s COM and core) and the inner separation of binary<sub>2–3</sub> (dashed lines) during the evolution. Both the separation between the COM of binary<sub>2–3</sub> (dotted lines) and the separation between its closest component to the core (solid lines) are shown. The wider inner-binary (binary<sub>2–3</sub>) is disrupted as it reaches the region of the core, whereas the binary<sub>2–3</sub> with the shorter-period (orange) remains bound, imparts more energy to the envelope expanding it and decreasing its density, until eventually it merges. Middle panel: The local density around the center of mass of binary<sub>2–3</sub>. We chose a sphere with a radius of  $50R_{\odot}$  to calculate the average density around binary<sub>2–3</sub>’s COM. The average density around the more compact binary<sub>2–3</sub> decreases more rapidly, although there is an apparent strong decrease of the density around the wider binary close to its merging point. At this stage, the location of the COM is farther from the dense region near the giant core, due to the binary disruption (see upper panel). Lower panel: The total gravitational force on the binary<sub>2–3</sub>. This force increases rapidly as the wider binary in-spirals to the core, while a slower evolution is seen for the more compact binary, due to its stronger dilution of the envelope throughout the in-spiral.

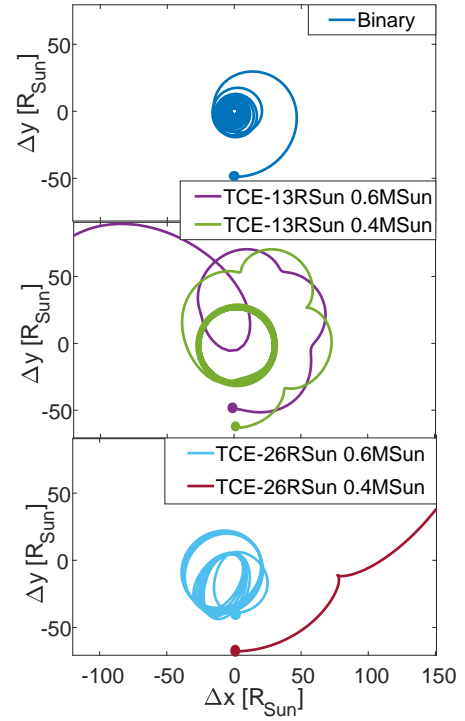


**Figure 13.** Comparison of the orbital evolution in a common envelope for triples with mass components  $2M_{\odot} + 0.6M_{\odot} + 0.4M_{\odot}$  of different inner binary<sub>2–3</sub> separations, and the CE evolution of the corresponding binaries of equivalent masses (simulations 12, 13 and 15 in Table 1). The first companion is  $0.6M_{\odot}$  compact object, whereas the second is  $0.4M_{\odot}$ .  $\Delta x$  and  $\Delta y$  are the difference in the location between the companion and the giant core in  $x$  and  $y$  coordinates. The dots mark the initial separation of the companion from the core.

Sim.	Inclination	$a_{in}$ ( $R_{\odot}$ )	Merged components	Merger time (days)
1	$5^{\circ}$	26	companion + core	289
2	$5^{\circ}$	3	binary <sub>2–3</sub>	706
3	$45^{\circ}$	26	companion + core	475
4	$45^{\circ}$	3	binary <sub>2–3</sub>	760
14	Binary		core merger	106

**Table 2.** Results summary of  $8M_{\odot} + 1M_{\odot} + 1M_{\odot}$  with  $0^{\circ}$  phase. All models here are initialized with the binary<sub>2–3</sub> located at a distance of 1AU from the giant core.

### 3.2 Binaries vs. triples

The general differences between TCEs and binary CEs can be studied by comparing simulations of triple systems and their corresponding binary systems, in which binary<sub>2–3</sub> is replaced by single star having the summed mass of the binary components, initially positioned at the COM of the original binary. Figure 14 shows the comparison of the evolution of the separation between the giant core and the companion

Sim.	Inclination	$a_{\text{in}}$ ( $R_{\odot}$ )	Merged components	Merger time (days)
7	$5^{\circ}$	26	companion + core	544
8	$5^{\circ}$	3	binary <sub>2-3</sub>	75
9	$45^{\circ}$	26	companion + core	85
10	$45^{\circ}$	3	binary <sub>2-3</sub>	5

**Table 3.** Results summary of  $8M_{\odot} + 1M_{\odot} + 1M_{\odot}$  with  $90^{\circ}$  phase. All models here are initialized with binary<sub>2-3</sub> located at a distance of  $0.6\text{AU}$  from the giant core.

Sim.	$a_{\text{in}}$ ( $R_{\odot}$ )	Ejected component	Ejection velocity ( $\text{km s}^{-1}$ )
12	13	$0.6M_{\odot}$	$\sim 95$
13	26	$0.4M_{\odot}$	$\sim 120$

**Table 4.** Results summary of the models with  $2M_{\odot} + 0.6M_{\odot} + 0.4M_{\odot}$  components, all with  $0^{\circ}$  inclination and orbital phase. In both separations considered, no merger between any of the components occurs during the simulation. In the case of the small separation of  $3R_{\odot}$  binary<sub>2-3</sub> merged very rapidly. Ejection velocities were measured upon leaving the envelope.

star/binary-COM for simulations 1 and 14. As can be seen, the TCE evolution extends longer than the binary CE evolution, although it appears that the evolution following the fast plunge-in is not significantly different. Similar conclusions can be obtained from Figure 13.

The fraction of unbound mass in our triple simulations, which is still much less than the entire envelope, was between 11 and 28 percent of the envelope mass, slightly larger than the unbound mass found in our binary simulation (number 14) which was around 10 percent.

## 4 DISCUSSION

Our results suggest TCE evolution in circumstellar configurations typically lead to either the merger of the components of binary<sub>2-3</sub> before it approaches the core; or the excitation of the orbit of binary<sub>2-3</sub> and eventually its disruption as it in-spirals closer to the core, leading to chaotic triple dynamics involving all three components (the components of binary<sub>2-3</sub> and the giant core), which are still embedded in the gaseous envelope. Following the chaotic evolution, the components of the disrupted binary can either mutually merge, one or both can merge with the core, or one of them may be ejected from the system. We briefly discuss each of these possibilities below.

As discussed above, the specific evolution of the TCE strongly depends on the particular triple configuration adopted, including the inner and outer binary separations, the mutual inclination between binary<sub>2-3</sub> and its orbit around the giant (binary<sub>1-23</sub>), and the masses of the components. We see that all of the parameters we investigated affect the triple common envelope process; its duration, the

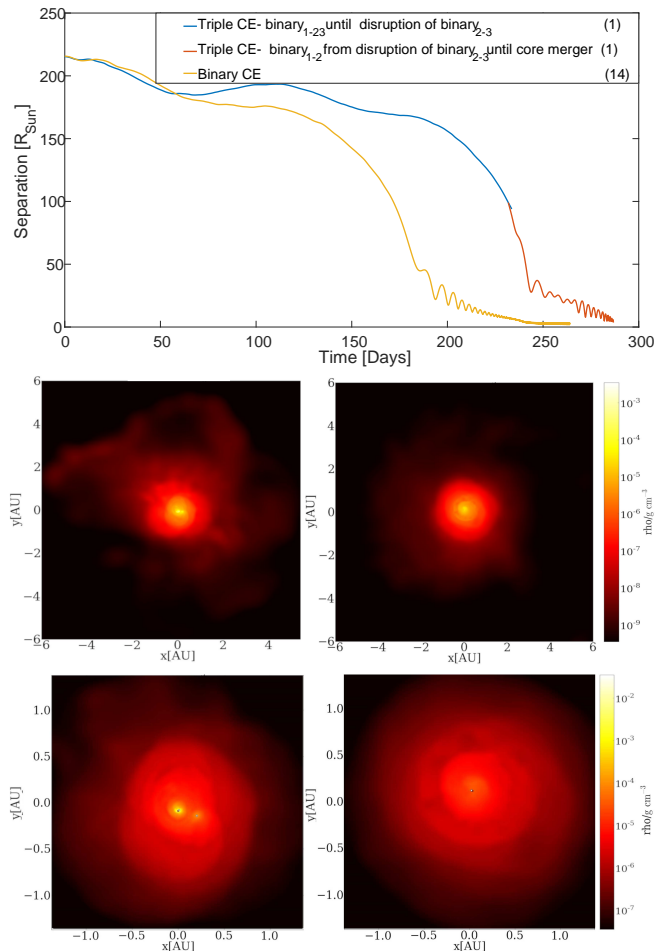


**Figure 14.** Comparison between the evolution of a triple system with  $8M_{\odot}$  giant with  $1M_{\odot} + 1M_{\odot}$  companions (simulation 1 in Table 1) and a corresponding binary system, consisting of a companion which is the sum of both components of binary<sub>2-3</sub> (simulation 14). Upper plot: the separation between the COM of binary<sub>2-3</sub> and the core, until the disruption of binary<sub>2-3</sub>'s components, follows by the separation between the companion to be merged with the core and the giant's core. Middle: snapshots that were taken at the end of simulations 1 and 14 in Table 1 from left to right, to demonstrate the different shape of the remnants. Bottom: same snapshots, but zoomed and different density scale. We can see that even the denser part of the envelope is much less symmetric in the left snapshot of the TCE, than the one on the right, of the parallel binary CE.

final result and even its final ejecta's observed shape. The results may have important implications for the formation and evolution of various types of compact binaries, their mergers and the possible electromagnetic and gravitational-wave transients they might produce.

### 4.1 Mergers

In our simulations, the exact nature of the components of binary<sub>2-3</sub> was not assumed, and they could potentially be either MS stars or compact objects. A compact binary<sub>2-3</sub> that is consisted of 2 MS stars, overflow their Roche-lobe while the orbit becomes tighter. In this case, modeling binary<sub>2-3</sub> as 2 point-mass stars is not accurate to explore their fate

accurately. However, if one is only interested whether they merge or not, this description is sufficient. We briefly discuss some of the more unique outcomes that may potentially arise from such evolutionary scenarios.

The merger of two MS stars could leave behind a blue straggler. Formation of blue-stragglers in triples were explored by us and others before (Perets & Fabrycky 2009; Perets & Kratter 2012; Naoz & Fabrycky 2014), but following very different evolutionary scenarios, and giving rise to different outcomes. In particular, if the merged star does not merge with the core during the CE, the post-CE binary (formerly triple) would become a unique binary - a potentially short-period blue-straggler binary, with a likely He-WD companion (or He-CO hybrid WD; Zenati et al. 2019), a configuration which is difficult to explain through other evolutionary scenarios. Interestingly, a binary He/hybrid-WD - blue-stragglers might have already been observed (Gosnell et al. 2014).

If the components of binary<sub>2-3</sub> are two white-dwarfs, the merger may leave behind a massive WD, that may later merge with the RG core during the CE, or survive and then potentially merge with the remnant of the RG core, likely a He-WD or hybrid He-CO WD (if they in-spiral through gravitational-wave emission). Such evolution might give rise to a type Ia supernova (Perets et al. 2019). Alternatively, the merger of binary<sub>2-3</sub> WD might result in type Ia supernova - (see also Di Stefano 2019) or form a different type of star (e.g. Stefano 2018). In such cases, the supernova would occur while still embedded in the CE. The strong shock interaction with the envelope might produce a long-lasting and more luminous supernova, possibly also related to the recently suggested origin of super-luminous supernovae from thermonuclear explosions inside a common envelope (Jerkstrand et al. 2020).

We note in passing, that in cases where binary<sub>2-3</sub> is composed of neutron stars or black holes, a TCE could induce their merger, leading to the production of gravitational-waves sources with unique signatures (e.g. somewhat similar to the cases of CE-induced gravitational-waves sources explored by us; Ginat et al. (2020)). However, the evolution of such massive components is not explored by our current models, and the study of whether a realistic evolutionary scenario can produce such cases is beyond the scope of the current work.

The result of a merger between one of the components of binary<sub>2-3</sub> and the RG core, leaves behind the second component, which can then continue to a second CE phase. Such evolution will form a new star with a larger mass than the original core, but smaller than the initial evolved giant. The exact nature of such rejuvenated red-giant (or possibly a Thorne-Zitkow, Thorne & Zytkow 1977; in case a neutron-star in-spirals to the core) is yet to be explored.

We should also note that in a somewhat different scenario of a resulting binary system, a further accretion could occur from the inner gas with its new formed core, on the other companion, suggested to form an X-Ray binary by Eggleton & Verbunt (1986). Further outcomes of the merger of binary<sub>2-3</sub> components have also been suggested and studied by Soker (2016); Hillel et al. (2017) and Soker (2019).

## 4.2 Ejections, runaway stars and single SdB stars

Due to the chaotic triple interaction between the components of binary<sub>2-3</sub> and the RG core, one of the components might

be ejected. Its typical velocity would be comparable to the orbital velocities at the point of the disruption of binary<sub>2-3</sub>, which can be as high as a few tens or even 100 km s<sup>-1</sup>. The TCE could therefore give rise to a novel channel for the production of runaway stars, albeit likely only in relative rare cases. In simulation 12 (see Table 1 for its configuration, Figure 13 for its orbit and Table 4 for the summary of results), the more massive companion was ejected with an initial (relative to the core) velocity of  $v_{dist} \approx 133 \text{ km} \cdot \text{s}^{-1}$ , and then went through the giant envelope, dissipating some of the velocity to reach a velocity of  $v_{ej} \approx 95 \text{ km} \cdot \text{s}^{-1}$  upon leaving the envelope. A simple calculation of its velocity without the effect of dynamical friction would give a velocity of about  $\sim 129 \text{ km} \cdot \text{s}^{-1}$ , higher than the measured velocity, showing the importance of the CE dissipation even during ejections. Ejections are therefore less likely, or give rise to lower ejection velocities when interacting with more massive envelopes. If the RG core is ejected (i.e the central core is ejected while the envelope material remains bound to the binary<sub>2-3</sub> or to one of its components), it might be observed as a single sdB star. Interestingly, single sdB stars are difficult to explain as such stars are typically expected (and observed; e.g. Geier et al. 2008) to have a close-by companion which took part in their formation through stripping their envelope. Though TCEs are unlikely to explain a high frequency of single sDBs, the finding of runaway single sDBs could provide a potential smoking gun signatures for such processes.

## 4.3 Planetary nebulae

Shortly after the end of the self regulating phase, any of the observed systems will consist of one or more compact objects, surrounded by the unbound gas as a planetary nebula. Planetary nebula could be the result of a post-AGB star that lost its envelope during late-evolution stages. However, the ejection of an AGB stellar envelope is likely to be spherically symmetric, thereby producing a symmetric planetary nebula, whereas the mass loss in common envelope evolution is mostly via the second and third Lagrangian points, both during the CE as well as during the interaction prior to this phase. The resulting planetary nebulae of such binary system is therefore not expected to be spherically symmetric, and could even sometimes be bipolar (De Marco et al. 2008; De Marco 2009; Miszalski et al. 2009; Jones et al. 2014; Jones, D. et al. 2015). Moreover, Zou et al. (2020) showed that even spherical outflows from the post-CE binary can be highly deflected by the interaction with the CE ejecta, and result in highly collimated bipolar outflows that may increase the asymmetry of the planetary nebula. As discussed above, TCE could give rise to highly aspherical and non axis-symmetric planetary nebulae, and the shape might not be ellipsoidal as in the post-CE binary cases, thereby giving rise to a wide diversity of shapes Soker et al. 1992; Soker 2016; Bear & Soker 2017).

## 4.4 Mass loss

Hydrodynamical simulations of binary CEE show that only a fraction of the envelope mass is ejected, while the majority (typically 90-80%) remains bound; (e.g. Passy et al. 2012; Ricker & Taam 2012; Ivanova et al. 2013, 2015; Kuruwita et al. 2016; Ohlmann et al. 2016; Iaconi et al.

2017), posing a potential problem, since these should result in a merger of the entire system instead of a compact post-CE binary. It was suggested that recombination energy can provide an additional energy source to drive the ejection of the envelope (Ivanova et al. 2015, and references therein). However, the fraction of the recombination energy lost to radiation is still debated (Soker & Harpaz 2003; Ivanova 2011; Clayton et al. 2017; Sabach et al. 2017; Grichener et al. 2018). Furthermore, the existence of wide post-CE orbits cannot be explained by merely including recombination energy (Reichardt et al. 2020). Others suggested that accretion energy mediated by jet/outflows may play a role (e.g. Shiber et al. 2019; Schreier et al. 2019, and references therein) or that dust formation inside the CE could drive winds and help to eject more material (Glanz & Perets 2018, and references therein) on longer timescales, with possible observational evidence for such long-term mass-loss (Michaely & Perets 2019; Igoshev et al. 2019). Our hydrodynamical simulations of a TCE evolution show that TCE also gives rise to inefficient mass-loss. However, as discussed above, the coupling of the binding energy of binary<sub>2-3</sub> to the envelope provides an additional energy/momentum source and leads to a longer in-spiral timescale, and a much larger mass-loss from the TCE, compared with the corresponding binary CEE cases. The unbound mass was calculated by the total mass of the SPH particles with  $e_{kin} + e_{pot} > 0$ , where  $e_{kin}$  and  $e_{pot}$  are the specific kinetic energy of the particle, with a velocity relative to the COM of the envelope, and an approximation of its gravitational potential due to the envelope. The gravitational potential energy between any two particles is calculated as follows:

$$E_{pot,ij} = -Gm_i m_j / r_{ij}$$

where  $m_i$ ,  $m_j$  are the masses of particles  $i$  and  $j$ , and  $r_{ij}$  is their separation. The potential energy of a particle is the sum over all particles potential in the system-

$$E_{pot,i} = \sum_j E_{pot,ij}.$$

Other works suggest the inclusion of the thermal energy of a particle in considerations of the ejected mass; however, this could only give an upper limit, as much of the thermal energy could be radiated away. Our models do not include radiative transfer and we do not consider the thermal energy in the mass-loss estimate. In any case, in this work, we do not try to solve the general problem of CE mass loss, but only compare between the different scenarios. Therefore, this approximation is applicable for our purposes. In the longest-lasting in-spiral we find a mass loss of  $\sim 27\%$ , compared with only  $\sim 8\%$  in the equivalent binary case. Moreover, our simulations terminate once two of the components merges (reach the sum of their radii), while the CE may proceed afterwards, and therefore the TCE mass loss fractions cited are only a lower-limit. Since only a fraction of CE cases involve triples, the more efficient TCE mass-losses cannot generally solve the envelope-ejection problem, but the more significant mass-loss do show an additional qualitative difference in the TCE evolution compared to binary CEE.

## 5 SUMMARY

In this study we have carried out the first hydrodynamical modeling of a triple common envelope evolution in a circumstellar configuration, where a more compact binary (termed binary<sub>2-3</sub> or the inner binary) orbits an evolved giant and eventually in-spirals into its envelope producing a TCE. We made use of the Gadget2 SPH code coupled to few-body codes using the AMUSE environment to combine the hydrodynamical aspects with the few-body dynamics involved. Given the computational expense we studied only a limited grid of models, serving as initial exploration of the sensitivity of the evolution to the initial orbital configurations, and the possible different outcomes of TCEs. We studied a total of 11 TCE models with different masses, inner-binary<sub>2-3</sub> separations, orbital, relative inclinations and orbital phases. We also compared our models with corresponding binaries, where binary<sub>2-3</sub> was replaced with a single component of the same total binary mass. We terminated the simulations once any two components merged during the simulation (the components of binary<sub>2-3</sub> and/or the RG-core).

We find that the TCE evolution leads to both the mutual in-spiral of the components of binary<sub>2-3</sub>, and their possible merger, as well as the in-spiral of binary<sub>2-3</sub> towards the red-giant core. We find that the more compact binary<sub>2-3</sub> configurations result in the mutual merger of the components of binary<sub>2-3</sub> before they approach the RG-core, while wider inner-binaries<sub>2-3</sub> do not merge, but in-spiral to the core and are then disrupted by the RG inner potential of binary<sub>2-3</sub>. In the latter case the (now unbound) components of binary<sub>2-3</sub> and the RG core evolve through chaotic triple dynamics, while still embedded in the envelope, leading to the merger of at least two of these components, and the possible ejection of the third.

The binary<sub>2-3</sub> provides an additional energy/momentum source, and its coupling to the envelope gives rise to stronger expansion of the envelope and significantly larger mass loss, but not substantial as to completely unbind the entire envelope. Consequently, the envelope density decreases more rapidly, and the timescale for the in-spiral towards the core is extended in comparison to the binary models. In addition, this evolution lives behind a significantly more aspherical and non axis symmetric remnant than the binary case (see bottom of Figure 14). We find that the specific evolution is sensitive to the initial configuration, but our models provide only a limited sample of the large phase space of triples, while a full characterization of the dependence is yet to be explored.

Our findings suggest that TCE can give rise to unique outcomes, and the possible production of peculiar blue-straggler binaries; unique gravitational-wave sources with gas-coupling dominated evolution (see also Ginat et al. 2020); potentially super-luminous peculiar thermonuclear supernovae (due to explosions following WD mergers inside the TCE); short-GRBs from neutron-stars mergers inside a TCE and the production of gravitational-wave sources; runaway stars (and possibly runaway SdBs); and other exotic mergers and their potential transient outcomes. Predicting the rates and branching ratios for the rich phase space of TCEs is beyond the scope of our exploratory study; and should be explored in the future.

## ACKNOWLEDGEMENTS

We greatly thank the referee, Orsola De Marco, for comprehensive and constructive comments. We thank Noam Soker for helpful discussions. HG and HBP acknowledge support for this project from the European Union's Horizon 2020 research and innovation program under grant agreement No 865932-ERC-SNeX.

We used the following codes in the simulations, analysis and visualizations presented in this paper: AMUSE (Portegies Zwart et al. 2009), MESA (version 2208) (Paxton et al. 2011), GADGET2 (Springel 2005), HUAYNO (Pelupessy et al. 2012), MI6 (Fujii et al. 2007), matplotlib (Hunter 2007), pynbody (Pontzen et al. 2013), NumPy (Harris 2020). All models were running on the Astric computer cluster of the Israeli I-CORE center.

## DATA AVAILABILITY

All data underlying this research is available upon reasonable request to the corresponding authors.

## REFERENCES

- Bear E., Soker N., 2017, *ApJ*, **837**, L10
- Clayton M., Podsiadlowski P., Ivanova N., Justham S., 2017, *mnras*, **470**, 1788
- De Marco O., 2009, *PASP*, **121**, 316
- De Marco O., Hillwig T. C., Smith A. J., 2008, *AJ*, **136**, 323
- Di Stefano R., 2019, in AAS/High Energy Astrophysics Division. AAS/High Energy Astrophysics Division. p. 112.72
- Eggleton P. P., Verbunt F., 1986, *MNRAS*, **220**, 13P
- Ford E. B., Kozinsky B., Rasio F. A., 2000, *ApJ*, **535**, 385
- Fujii M., Iwasawa M., Funato Y., Makino J., 2007, *Publications of the Astronomical Society of Japan*, **59**, 1095
- Geier S., Karl C., Edelmann H., Heber U., Napiwotzki R., 2008, Binary sdB Stars with Massive Compact Companions. Astronomical Society of the Pacific Conference Series, p. 207
- Ginat Y. B., Glanz H., Perets H. B., Grishin E., Desjacques V., 2020, *MNRAS*, **493**, 4861
- Glanz H., Perets H. B., 2018, *MNRAS*, **478**, L12
- Gosnell N., Mathieu R., Geller A., Sills A., Leigh N., Knigge C., 2014, *The Astrophysical Journal Letters*, **783**
- Grichener A., Sabach E., Soker N., 2018, *MNRAS*, **478**, 1818
- Hamers A. S., Pols O. R., Claeys J. S. W., Nelemans G., 2013, *MNRAS*, **430**, 2262
- Hillel S., Schreier R., Soker N., 2017, *MNRAS*, **471**, 3456
- Iaconi R., Reichardt T., Staff J., De Marco O., Passy J.-C., Price D., Wurster J., Herwig F., 2017, *mnras*, **464**, 4028
- Iben Icko J., Tutukov A. V., 1999, *ApJ*, **511**, 324
- Igoshev A. P., Perets H. B., Michaely E., 2019, arXiv e-prints, p. arXiv:1907.10068
- Ivanova N., 2011, in Schmidtobreick L., Schreiber M. R., Tappert C., eds, Astronomical Society of the Pacific Conference Series Vol. 447, Evolution of Compact Binaries. p. 91 (arXiv:1108.1226)
- Ivanova N., et al., 2013, *aapr*, **21**, 59
- Ivanova N., Justham S., Podsiadlowski P., 2015, *mnras*, **447**, 2181
- Izzard R. G., Hall P. D., Tauris T. M., Tout C. A., 2012, in IAU Symposium. pp 95–102
- Jerkstrand A., Maeda K., Kawabata K. S., 2020, *Science*, **367**, 415
- Jones, D. Boffin, H. M. J. Rodríguez-Gil, P. Wesson, R. Corradi, R. L. M. Miszalski, B. Mohamed, S. 2015, *A&A*, **580**, A19
- Jones D., Boffin H. M. J., Miszalski B., Wesson R., Corradi R. L. M., Tyndall A. A., 2014, *A&A*, **562**, A89
- Kuruwita R. L., Staff J., De Marco O., 2016, *mnras*, **461**, 486
- Michaely E., Perets H. B., 2014, *ApJ*, **794**, 122
- Michaely E., Perets H. B., 2019, *MNRAS*, **484**, 4711
- Miszalski B., Acker A., Parker Q. A., Moffat A. F. J., 2009, *A&A*, **505**, 249
- Moe M., Di Stefano R., 2017, *ApJS*, **230**, 15
- Monaghan J. J., 1992, *araa*, **30**, 543
- Naoz S., 2016, *ARA&A*, **54**, 441
- Naoz S., Fabrycky D. C., 2014, *ApJ*, **793**, 137
- Ohlmann S. T., Röpke F. K., Pakmor R., Springel V., 2016, *apjl*, **816**, L9
- Paczynski B., 1976, in Eggleton P., Mitton S., Whelan J., eds, IAU Symposium Vol. 73, Structure and Evolution of Close Binary Systems. p. 75
- Passy J.-C., et al., 2012, *apj*, **744**, 52
- Paxton B., Bildsten L., Dotter A., Herwig F., Lesaffre P., Timmes F., 2011, *ApJS*, **192**, 3
- Pelupessy F. I., Jänes J., Portegies Zwart S., 2012, *New Astron.*, **17**, 711
- Perets H. B., Fabrycky D. C., 2009, *ApJ*, **697**, 1048
- Perets H. B., Kratter K. M., 2012, *apj*, **760**, 99
- Perets H. B., Zenati Y., Toonen S., Bobrick A., 2019, arXiv e-prints, p. arXiv:1910.07532
- Portegies Zwart S., Leigh N. W. C., 2019, *ApJ*, **876**, L33
- Portegies Zwart S., McMillan S., 2018, *Astrophysical Recipes*. 2514-3433, IOP Publishing, doi:10.1088/978-0-7503-1320-9, http://dx.doi.org/10.1088/978-0-7503-1320-9
- Portegies Zwart S., et al., 2009, *New Astron.*, **14**, 369
- Reichardt T. A., De Marco O., Iaconi R., Tout C. A., Price D. J., 2019, *MNRAS*, **484**, 631
- Reichardt T. A., De Marco O., Iaconi R., Chamandy L., Price D. J., 2020, *MNRAS*, **494**, 5333
- Ricker P. M., Taam R. E., 2012, *apj*, **746**, 74
- Sabach E., Soker N., 2015, *MNRAS*, **450**, 1716
- Sabach E., Hillel S., Schreier R., Soker N., 2017, *MNRAS*, **472**, 4361
- Schreier R., Hillel S., Soker N., 2019, *MNRAS*, **490**, 4748
- Shappee B. J., Thompson T. A., 2013, *ApJ*, **766**, 64
- Shiber S., Iaconi R., De Marco O., Soker N., 2019, *MNRAS*, **488**, 5615
- Soker N., 2004, *MNRAS*, **350**, 1366
- Soker N., 2016, *MNRAS*, **455**, 1584
- Soker N., 2017, *MNRAS*, **471**, 4839
- Soker N., 2019, arXiv e-prints, p. arXiv:1912.01550
- Soker N., 2020, arXiv e-prints, p. arXiv:2002.04229
- Soker N., Harpaz A., 2003, *MNRAS*, **343**, 456
- Soker N., Zucker D. B., Balick B., 1992, *AJ*, **104**, 2151
- Springel V., 2005, *MNRAS*, **364**, 1105
- Hunter J. D., 2007, *IEEE*, **9**, 90
- Charles R. Harris and K. Jarrod Millman and St'efan J. van der Walt and Ralf Gommers and Pauli Virtanen and David Cournapeau and Eric Wieser and Julian Taylor and Sebastian Berg and Nathaniel J. Smith and Robert Kern and Matti Pícus and Stephan Hoyer and Marten H. van Kerkwijk and Matthew Brett and Allan Haldane and Jaime Fern'andez del R'io and Mark Wiebe and Pearu Peterson and Pierre G'erard-Marchant and Kevin Sheppard and Tyler Reddy and Warren Weckesser and Hameer Abbasi and Christoph Gohlke and Travis E. Oliphant, 2020, *Nature*, **585**, 357
- Stefano R. D., 2018, Mass from a third star: transformations of close compact-object binaries within hierarchical triples (arXiv:1805.09338)
- Pontzen A., Roškar R., Stinson G., Woods R., 2013, ascl.soft.1305.002
- Tauris T. M., van den Heuvel E. P. J., 2014, *The Astrophysical Journal*, **781**, L13
- Thompson T. A., 2011, *ApJ*, **741**, 82
- Thorne K. S., Zytlow A. N., 1977, *ApJ*, **212**, 832

- Toonen S., Hamers A., Zwart S. P., 2016, The evolution of hierarchical triple star-systems ([arXiv:1612.06172](https://arxiv.org/abs/1612.06172))
- Valtonen M., Karttunen H., 2006, The Three-Body Problem. Cambridge University Press, [doi:10.1017/CBO9780511616006](https://doi.org/10.1017/CBO9780511616006)
- Zenati Y., Toonen S., Perets H. B., 2019, *MNRAS*, **482**, 1135
- de Vries N., Portegies Zwart S., Figueira J., 2014, *mnras*, **438**, 1909
- Zou Y., Frank A., Chen Z., Reichardt T., De Marco O., Blackman E. G., Nordhaus J., 2020, *MNRAS*, **497**, 2855

This paper has been typeset from a  $\text{\TeX/L}^{\text{A}}\text{\TeX}$  file prepared by the author.